frontiers in Earth Science

ORIGINAL RESEARCH
published: 12 July 2021
doi: 10.3389/feart.2021.702828

Inferring Airflow Across Martian Dunes From Ripple Patterns and Dynamics

D. R. Hood[1,2], R. C. Ewing[2], K. P. Roback[3], K. Runyon[4], J.-P. Avouac[3] and M. McEnroe[2]*

[1]Department of Geosciences, Baylor University, Waco, TX, United States, [2]Department of Geology and Geophysics, Texas A&M University, College Station, TX, United States, [3]Division of Geological and Planetary Sciences, Caltech University, Pasadena, CA, United States, [4]Johns Hopkins University, Applied Physics Lab, Laurel, MD, United States

Large ripples form striking patterns on the slopes of martian sand dunes which can be mapped and tracked using high-resolution optical images. The ripples vary in orientation, wavelength, plan-view morphology, and rates of migration. The variations in the ripple patterns are recognized to signal the effects of the regional and local winds and feedbacks between winds and dune topography. We examine the ripple patterns and the motion of these ripples to interpret airflow dynamics around dunes in the dune field at Nili Patera. We find that coincident changes in ripple patterns and migration rates in dune wakes indicate reattachment lengths of 4–7 brink heights. This reattachment length is similar to length scales of flow reattachment for airflow over dunes measured on Earth despite the differences in aeolian environment. Furthermore, ripples on dune flanks are shown to behave according to terrestrial models for ripple development on steep slopes. Compensating for these slope effects allows them to act as indicators of dune-modified and regional wind directions. Changes in ripple patterns and migration rates also signal the response of dunes and airflow during dune collisions. Collectively, we find that differences in ripple patterns connected to changes in migration rate provide information on airflow over and around dunes. This detailed assessment of ripple measurement and ripple migration rates advances the use of ripples on martian dunes and sand sheets to infer dune- and field-scale wind dynamics. These measurements also indicate that the low density atmosphere on Mars does not significantly modify the behavior of wind-topography interactions compared to Earth. Such observations provide targets for computational fluid dynamic and large-eddy simulation models seeking to reveal complex airflows across dune fields both on Earth and on Mars.

Keywords: mars, ripple activity, HiRISE images, flow topography interaction, dunes

OPEN ACCESS

Edited by:
Simone Silvestro, Astronomical Observatory of Capodimonte (INAF), Italy

Reviewed by:
David Vaz, University of Coimbra, Portugal
Charles Bristow, Birkbeck, University of London, United Kingdom

****Correspondence:***
D. R. Hood
drhood2938@gmail.com

Specialty section:
This article was submitted to Quaternary Science, Geomorphology and Paleoenvironment, a section of the journal Frontiers in Earth Science

Received: *30 April 2021*
Accepted: *23 June 2021*
Published: *12 July 2021*

Citation:
Hood DR, Ewing RC, Roback KP, Runyon K, Avouac J-P and McEnroe M (2021) Inferring Airflow Across Martian Dunes From Ripple Patterns and Dynamics. Front. Earth Sci. 9:702828. doi: 10.3389/feart.2021.702828

INTRODUCTION

Meter-scale ripples cover sand dunes on Mars (Schatz et al., 2006; Bridges et al., 2007; Ewing et al., 2010; Silvestro et al., 2010; Chojnacki et al., 2011; Bridges et al., 2012; Liu and Zimbelman., 2015; Lapotre et al., 2016; Runyon et al., 2017; Roback et al., 2020). The origin of these anomalously large ripples is debated (Lapotre et al., 2016; Lapotre et al., 2018; Vinent et al., 2019; Lorenz et al., 2020; Sullivan et al., 2020; Lapotre et al., 2021), but similar to cm-scale ripples covering dunes on Earth, these ripples are a signal of modern winds blowing across the dunes (Ayoub et al., 2014; Silvestro

et al., 2016; Ewing et al., 2017; Vaz et al., 2017). Dune patterns, in addition to ripple patterns where visible, serve as a first-order means to interpret wind patterns on Mars and other worlds (Lorenz et al., 2006; Jia et al., 2017; Telfer et al., 2018), as validation for rover studies (e.g., Ewing et al., 2017; Newman et al., 2017), and as targets for numerical simulations (Runyon et al., 2017). However, unlike on other bodies, both martian dunes and ripple patterns are visible in satellite images, which allows detailed observation and mapping of ripple patterns across dunes. In turn, this affords the opportunity to assess wind flows across dunes and through dune fields in a manner not feasible via satellite remote sensing on Earth. These observations can improve understanding of meteorological patterns on Mars (Ayoub et al., 2014) and reduce uncertainty associated with winds affecting landing or launch crafts.

Ripple patterns on dunes have long been recognized as indicators of wind fields across dunes (Bagnold, 1941; Cooper, 1958; Wilson, 1971, Howard et al., 1977; Kocurek et al., 2007), however, on Earth they have not been widely used as a primary means to assess airflow across dunes due to the difficulty in mapping cm-scale ripples over meter-to-kilometer-scale dunes. More typically, assessing wind flows across dunes on Earth has been done using direct field observations of winds or, more recently, experiments and computer simulations of flow fields. Time and equipment intensive field studies have typically employed mast-mounted anemometers to characterize the wind fields (Lancaster, 1985; Frank and Kocurek, 1996a,b; Wiggs et al., 1996; Neuman et al., 1997; Walker et al., 2002; Baddock et al., 2011; Claudin et al., 2013). Sophisticated laboratory experiments and numerical simulations are increasingly used to characterize wind flows over dunes and through dunes fields (Parsons et al., 2004; Wang and Anderson, 2019; Zgheib et al., 2018a; Zgheib et al., 2018b; Bristow et al., 2018; Bristow et al., 2019; Bristow et al., 2020). These field measurements, laboratory experiments, and numerical simulations have served to identify important, primary characteristics of winds moving across and interacting with dune topography on Earth, but less is known about how winds respond to dune topography on Mars where the atmospheric density is sixty times less than on Earth.

The basic structure of winds blowing across dunes identified though observations and models in early studies remains relevant for most geomorphological studies despite an increasing understanding of the complexities of turbulence and its role in dune field evolution (e.g., Zgheib et al., 2018a, Zgheib et al., 2018b). The flow is compressed as the wind feels the topography of the dune stoss slope and accelerates to the dune crest (**Figure 1A**) (Jackson and Hunt, 1975; Bennet and Best, 1995; Frank and Kocurek, 1996; Baddock et al., 2011; Smith et al., 2017)). Flow separation and flow decompression occurs as flows move past the sharp break in slope at the dune brink. A recirculation cell forms in the dune wake marked in its downwind extent by a reattachment point and returns flow toward the dune lee at a distance related to the dune shape and height (Baddock et al., 2011). Downwind of the flow reattachment point, an internal boundary layer develops and grows as flow recovers to the overlying flow. This dune-modified flow scenario varies with wind flows from different directions and intensities, with dune shape, and with proximity to other dunes (Baddock et al., 2011; Zgheib et al., 2018a, Zgheib et al., 2018b, Bristow et al., 2020). Dune-modified flows affect dune shape, control the type and distribution of lee slope sedimentation processes (Eastwood et al., 2012; Swanson et al., 2016; Lee et al., 2019), and play an influencing role in dune interactions in which an upwind dune approaches and may collide with a downwind dune (Bristow et al., 2018; Wang and Anderson, 2019; Assis and Franklin, 2020; Bacik et al., 2020). Despite recognition of the role of dune modified flows in shaping dunes and affecting their migration on Earth, few studies assessed the role of dune-modified flows on dune fields on Mars where such interactions are readily examined with remote sensing data.

A few studies of dunes and ripples on Mars inferred wind flow patterns across dunes using ripple patterns (**Figure 1B**) (Ewing et al., 2010; Jackson et al., 2015; Li and Zimbelman, 2015; Runyon et al., 2017). Ewing et al. (2010) mapped ripple orientations across dunes in Olympia Undae Dune Field. At the dune scale, the ripple patterns were oriented in a way that reflected expected airflow patterns across the dune brink. Lee side cross-hatch ripple patterns were interpreted as occurring in the lee-side recirculation cell. Ripples oriented perpendicular to the brink were interpreted as the result of along-slope flow from flow deflection by the dune topography. Reorientation of the ripples to a field-wide average was interpreted as flow recovery to a regional wind direction. These inferred flow patterns were supported by observations of lee slope sedimentation as rippled, grainfall, and grainflow structures that vary with the incidence angle of the flow to the brink (e.g., Eastwood et al., 2012). Jackson et al. (2015) modeled incident winds and dune-flow interaction at high resolution in a dune field in Proctor Crater, Mars, and compared the modeled winds to observed ripple motion within the field. Ripple motion in different areas within the dune field were found to correlate with different incident winds, but all areas were found to exhibit significant steering of flow by the dune topography. This demonstrates that locally steered flows are strong enough to transport sand in the martian environment, and in some cases such flows are more influential on the ripple motion than the regional wind direction.

In this study, we expand on prior studies by both mapping ripple patterns and their migration rates in the Nili Patera dune field. We also examine closely 2-D ripples on steep slopes as independent indicators of flow direction on dune flanks. From these observations we extract new details of airflow across dunes on Mars including flow reattachment and flow recovery length scales and flow deflection by upwind dunes.

MATERIALS AND METHODS

Dataset and Study Area

The Nili patera dune field is among the most active, well-studied dune fields on Mars with an inferred unidirectional wind regime (Bridges et al., 2012; Ayoub et al., 2014; Chojnacki et al., 2019; Roback et al., 2020). These attributes have resulted in the collection of an abundance of repeat HiRISE data, which

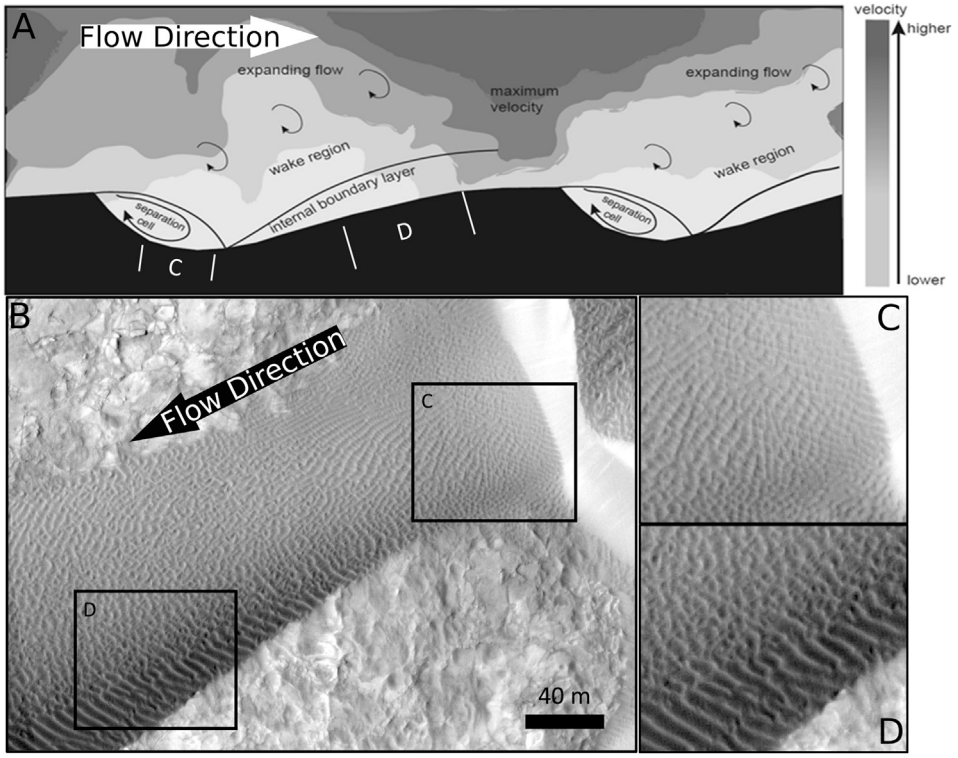

FIGURE 1 | Models of flow over dunes **(A)** with ripple patterns that may be connected to different regimes of flow **(B–D)**. The ripple pattern in **(C)** typifies the patterns seen in dune wakes: subdued, near isotropic patterns with evidence for primary ripple development with crests extending from the base of the slipface and superposed secondary ripple development parallel to the slipface. The patterns in **(D)** typify dune-top ripples **(upper left)** and 2-D ripples on a dune flank **(lower right)**.

TABLE 1 | HiRISE images used to generate ripple migration maps *via* COSI-Corr analysis. Solar Longitudes (Ls) are given for each image to express both the time difference between images and the season represented by each timestep. All images are of the format ESP_######_1890.

Map	Image 1	Image 2	L_s 1	L_s 2	Δ L_s	Δ days
028575	028575	028931	163.7	179	15.3	27
028931	028931	029643	179	211.5	32.5	56
029643	029643	030210	211.5	239.1	27.6	44
030210	030210	030843	239.1	270.3	31.2	49
032056	032056	032623	326.7	350.3	23.6	44
033045	033045	033546	6.8	25.4	18.6	39
033546	033546	034179	25.4	47.7	22.3	49
034179	034179	034680	47.7	64.9	17.2	39
034680	034680	035603	64.9	96.5	31.6	72
036091	036091	036447	113.6	126.6	13	28
036447	036447	037792	126.6	180.9	54.3	105

allows tracking of ripple migration using COSI-Corr (LePrince et al., 2007; Bridges et al., 2012; Ayoub et al., 2014). Importantly, because the winds are thought to be unidirectional, the ripples can be reliably used as wind indicators, which is not always the case because large ripples can integrate winds across seasonal cycles resulting in oblique and longitudinal ripple patterns (Jackson et al., 2015; Silvestro et al., 2016; Ewing et al., 2017). The resulting dataset at Nili Patera is among the highest fidelity image and ripple tracking datasets available on Mars, which facilitated the detailed examination of ripple patterns and migration rates on the dunes in this study.

We used HiRISE images and digital terrain models (McEwen et al., 2007) to map and analyze the ripple patterns (**Figure 1**). We used existing ripple migration data derived from COSI-Corr (Roback et al., 2020) to correlate ripple patterns with ripple migration (**Table 1**). The COSI-Corr method uses repeat images and DTMs to make precise measurements of ripple displacement on the dunes at spatial resolutions of ~5 m. The details of the COSI-Corr method for deriving ripple migration are described in Bridges et al. (2012) and Ayoub et al. (2014). Similar to prior work (Bridges et al., 2012), a bedrock-only DTM was generated from the regional HiRISE DTM to extract individual dune heights. Gaps in the DEM, where dunes were removed, were interpolated using a tension spline (weight = 10, N_points = 12).

Several study sites within the dune field were chosen to analyze the relationship between ripple migration and ripple patterns (**Figure 2**). Three sites (**Figure 2 A–C**) were chosen to analyze ripples in the wakes of dunes. The selection criteria for these dunes included upwind-downwind dune pairs with continuous sand cover, dunes with minimal upwind obstructions, and dunes that occur along an upwind-to-downwind transect through the dune field. Multiple transects were selected along the profile of each dune pair oriented parallel to the ripple migration direction. Along these transects, elevation, dune height (elevation—bedrock

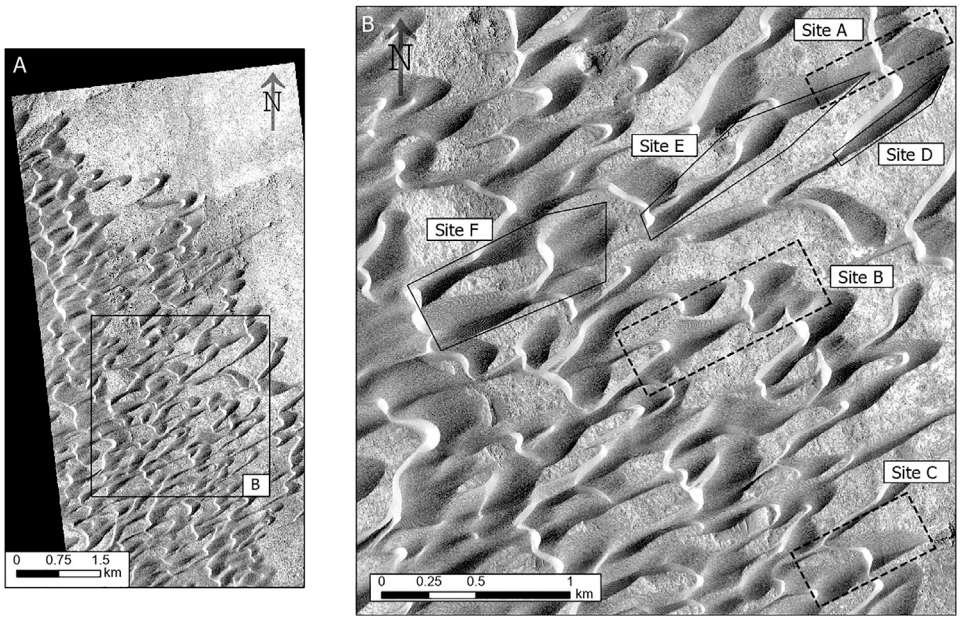

FIGURE 2 | HiRISE image of our study area **(A)** including the immediate vicinity of our study sites **(B)**. Sites A-C, outlined in dashed rectangles, are primarily used in investigations of wake flow (*Ripple Migration Rates on Dunes*), and areas outlines in solid polygons (D–F) are primarily used in investigations of 2-D ripples on dune flanks (*Wind Orientation*).

DEM model), ripple migration rate, and ripple patterns were examined. At sites A–C, dune surfaces were mapped into four categories: 3-Dimensional Dune-Top Ripples, 2-Dimensional linear ripples, Slipfaces, and Wake Ripples (**Figure 1**). In addition, two corridors were chosen along the dune field in which to study the wind-direction on slopes bearing 2-D ripples. These areas were chosen for the continuous presence of 2-D ripples across a transect through the dune field. These selection criteria resulted in relatively few sites but helped focus the study on sites with the highest fidelity to extract detailed insights into the dune-modified wind flows with minimal influence from other modifications to wind flow.

Determining Wind Direction From Ripple Orientation

In aeolian environments, ripples can act as robust indicators of flow direction. For unidirectional wind flows over flat surfaces, the direction orthogonal to the orientation of the ripple indicates the formative wind direction. On sloped surfaces, such as those on the sloped flanks of aeolian dunes, the relationship between formative wind directions and ripple orientation is more complex (Howard, 1977; Rubin, 2012). 2-D ripples are common on the sloped flanks of martian dunes and are used here to assess the relative role of regional winds and dune modified winds. Ripples on sloped surfaces have been found to be systematically and predictably deflected downslope depending on the direction and steepness of the slope, according to **Eq. 1** (Howard, 1977).

$$\sin(\beta) = \frac{\tan(\theta)}{\tan(\alpha)} \sin(\gamma) \quad (1)$$

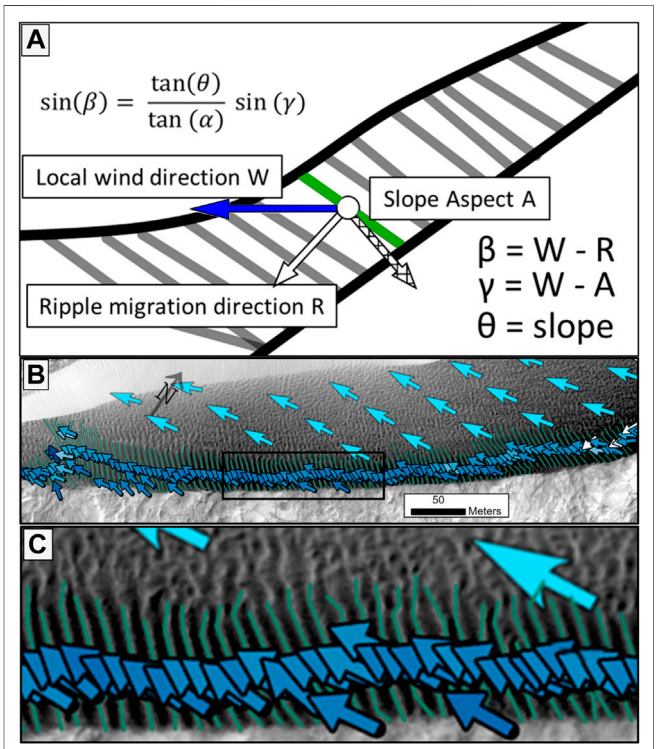

FIGURE 3 | (A) A visual expression of the Howard Equation (**Eq. 1**), **(B)** study site D with COSI-Corr derived ripple motion on the dune top (light blue arrows) and ripple traces (green) with interpreted wind direction (blue arrows), **(C)** detail of panel B.

In **Eq. 1**, β is the angle between the wind-direction and the ripple crest normal direction, θ is the slope of the surface, γ is the angle between the wind-direction and slope aspect, and α is the angle of repose (**Figure 3**). This equation predicts the deviation between formative wind direction and ripple orientation (β) to scale with the deviation between the formative wind direction and slope aspect (γ) modified by the ratio of the slope (θ) to the angle of repose (α). The derivation of this equation is independent of many aeolian parameters such as grain density, air density, and gravity and thus should be independent of changes in those parameters. One way in which the equation may be altered for application to Mars, is a change in the angle of repose, α, though the angle of repose on for dune sand on Mars has been shown to be similar to that of dune sand on Earth (Atwood-Stone and McEwen, 2013; Ewing et al., 2017). Grain properties can affect this angle, but such grain properties are likely relatively homogenous on active slopes within a dune field (Weitz et al., 2018) resulting in a constant angle of repose within the study area. In this investigation, results for $\alpha = 26^{\circ}$, 28°, and 30° will be considered as a range of possible solutions, which covers the range measured on Mars (Atwood-Stone and McEwen, 2013).

On the areas selected for 2-D ripple analysis (**Figure 2**, Sites D-G), we used **Eq. 1** to determine the formative wind direction of 2-D ripples on steep slopes. Each ripple crest was manually traced in ArcGIS, and polylines were used to determine the ripple orientation and crest-normal direction. Because **Eq. 1** was developed based on observations of ripple orientation, not ripple migration direction, these crest-normal directions will be used as inputs to **Eq. 1** rather than COSI-Corr derived migration directions. The ripple polyline was also used as the shape reference for the zonal statistics tool which determined the average slope, and slope aspect. Finally, we used a python script to solve for the wind direction that satisfied **Eq. 1** for each ripple.

RESULTS

Dune Field Patterns

The dune field at Nili Patera consists of sediment availability-limited asymmetric barchan and barchanoid ridges that transition from isolated dunes at the upwind margin downwind into interacting barchan dunes before becoming more continuous barchanoid ridges toward the center of the field. The barchan dunes are asymmetrical in which southern arms appear more elongate than the northern arms. Most dunes have typical crescentic shapes with defined stoss slopes and well developed grain avalanche-covered slipfaces. Rarely, elongate arms are detached from the host barchan thereby creating a linear ridge or dune finger (e.g., Courrech du Pont, 2014; Lucas et al., 2015). Interdune areas are bedrock and only occur as sediment-covered interdune troughs where barchanoid ridges form ~3 km from the upwind margin.

The dune asymmetry and dune collisions give rise to a wide range of dune interactions. Though the time series of images is not long enough to capture complete interactions, types and stages of interactions can be inferred from the images as a snapshot in time (e.g., Ewing et al., 2010). The types of dune interactions that occur in the field include lateral linking, merging, and off-center collisions (**Figure 2B**) (Ewing and Kocurek, 2010; Kocurek et al., 2010; Assis and Franklin, 2020; Bacik et al., 2020). Off-center collisions are the most abundant interaction facilitated by the barchan asymmetry and elongated barchan horns. The elongated horns or arms extend downwind and intersect the stoss slope of another barchan dune where they merge with the stoss slope of the downwind dune or, in some instances, develop their own slipface (**Figure 2B**, site E). Some off-center collisions and merging occur where the bodies of the barchan dunes collide. Lateral linking is apparent where the arms of the barchan dunes merge into a single shared arm. Though not an interaction, per se, rarely, spurs (e.g., Swanson et al., 2018) emerge from the barchan dune slipface and elongate downwind where they intersect other dunes. The spatial changes in dune patterns in the dune field and the abundance and nature of the interactions provide a means to assess how ripple patterns and migration rates are modified by airflow moving over and around dunes.

Three pairs of dunes met the site selection criteria (**Figures 4–6**). Site A is at the upwind margin of the field and retains structure from 3-4 merged dunes. A lee-side spur extends from a relatively low-elevation portion of the brink in the middle of the merged upwind dune. The trailing dune in this pair is longer and has a rounded crest compared to the leading dune but reaches similar overall height near the crest. The trailing dune also shows well-developed 2-D ripples on the flanks. Site B also retains evidence of a dune merger in the leading dune, and the trailing dune extends from the wake of the smaller of the merged dunes. The trailing dune in site B is taller than the leading dune, and shows a similar rounded structure to the trailing dune in site A. The dune pair at site C is more asymmetric than the other sites due to an upwind obstruction, but the obstruction does not appear to affect ripple migration rates and the trailing dune shows similar morphology to trailing dunes at the other sites.

Ripple Patterns on Selected Dunes

Ripples were readily identifiable and mappable at all sites as 2-D, 3-D, or wake-zone ripples. 2-D ripples are meters-long, straight, continuous ripple crests and are found on the steeper-sloped flanks of dunes. The transition from 2-D ripples to 3-D ripples is sharp with abrupt changes in slope, but poorly defined with gradual slope changes. In cases of gradual slope change, individual 2-D ripples extend meters into the 3-D ripples dominated areas. 3D ripples are sinuous, laterally discontinuous, and most common on the lower-slopes of the dune stoss slope. Immediately downwind of the dune brink, which would be in the wake flow coming across the dune brink, a variety of ripple patterns exist including linear ripples that extend normal to the slipface, nearly isotropic box-like ripples, and palimpsest 3-D ripples.

Two-dimensional ripples were mapped at three sites within the dune field (**Figure 2** sites D-F). The ripples are best developed where dune flanks exceed ~20° slope. Sites D and E are downwind of relatively wide inter-dune exposures of bedrock, which reduces the presence of upwind perturbations that could affect the ripple patterns. In contrast, site F is immediately downwind of several

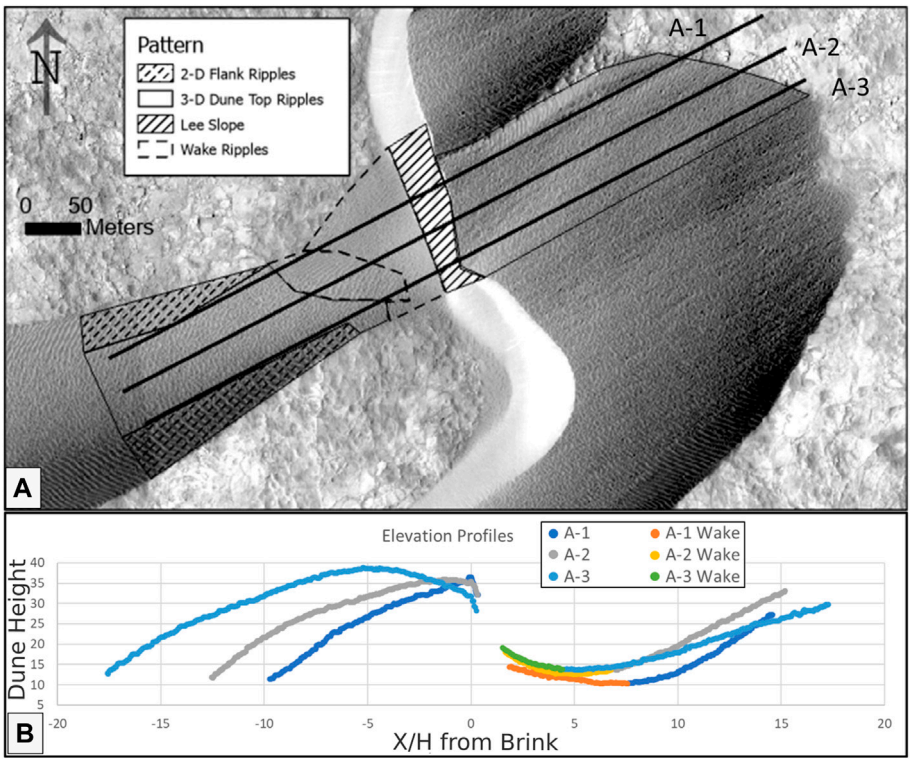

FIGURE 4 | Image of Dune A with ripples and transects mapped. Elevation along each transect is shown in the lower right corner, with lee slopes removed for clarity and areas mapped as "Wake Ripples" highlighted in the profile. The distance from the brink is measured positive in the downwind direction.

dunes, so the well-developed ripples there may record more complex flows.

Ripple Migration Rates on Dunes

Stoss Slopes

A linear relationship is expected between ripple migration rate (R) and height (H) on both leading and trailing dunes and has been reported in prior studies (Bridges et al., 2012; Runyon et al., 2017). To confirm this expectation and investigate deviations from this relationship, the migration rate (R), and migration rate to dune height ratio (R/H) were examined at 1-m intervals along transects at each dune pair (study sites A-C, **Figure 7**). **Figure 7** plots R/H observations in terms of the X-location relative to the brink ratioed to brink height (X/H). In these plots, negative X/H values indicate locations upwind of the brink of the first dune, and positive values indicate locations downwind of the brink.

Our results show the predicted linear relationship between ripple migration rate and dune height generally holds on dune stoss slopes. This relationship is shown in **Figure 7** where the R/H curve maintains a constant value along the transect within <5 brink heights of the base of the stoss slope in leading dunes. For example, in study sites B and C (**Figure 7 B, C**), all transects begin between −10 and −8 X/H and reach a constant value of ~0.3 R/H near −5 X/H. For study site A, the stoss slopes show an initially low R/H (**Figure 7A**) and start at varying distances from the brink, but all plateau within ~2 brink heights of the stoss slope base. Trailing dunes show a similar pattern when measured from the boundary of the wake-zone ripples to the 3D ripples, though the R/H curve reaches a constant value at varying distances from the wake-zone to 3-D ripple transition. Because transects were drawn parallel to the ripple migration direction, they do not extend all the way to the second dune brink in sites A and B. One transect was taken parallel to the dune morphology in site A to explore R/H patterns further along the second dune and confirm that the linear relationship is re-established on the trailing dune (**Figure 8**). In **Figure 8**, a stable R/H is reached at ~17 X/H, 10 brink heights from the wake-zone to 3-D ripple boundary. At sites B and C (**Figure 7 B, C**), the trailing dune stoss slope reaches a level R/H value within the transects, in both cases ~5 brink heights past the wake-zone to 3-D ripple boundary. Examination of stoss slopes at study sites A-C show that the expected linear R-H relationship is present, though this relationship gradually becomes established along a dune stoss slope over the first 5–10 brink heights and is established more gradually on trailing dunes. These patterns set the expectation for ripple migration rates on dune stoss slopes and help to identify any anomalous patterns within dune wake zones.

Wake Zones

Wake ripples (contrasting colors in **Figures 7**, **9**) showed deviations from the expected linear relationship between R and H. The wake zone in Dune A shows a trend of increasing R/H that extends between 4 and 7 brink heights from the dune brink. Along all transects except A-3, R/H decreases after the transition into 3-D ripples between 5 and 7 brink heights from the dune brink. In A-3, R/H reaches a plateau at ~6 X/H, though the transition into 3-D

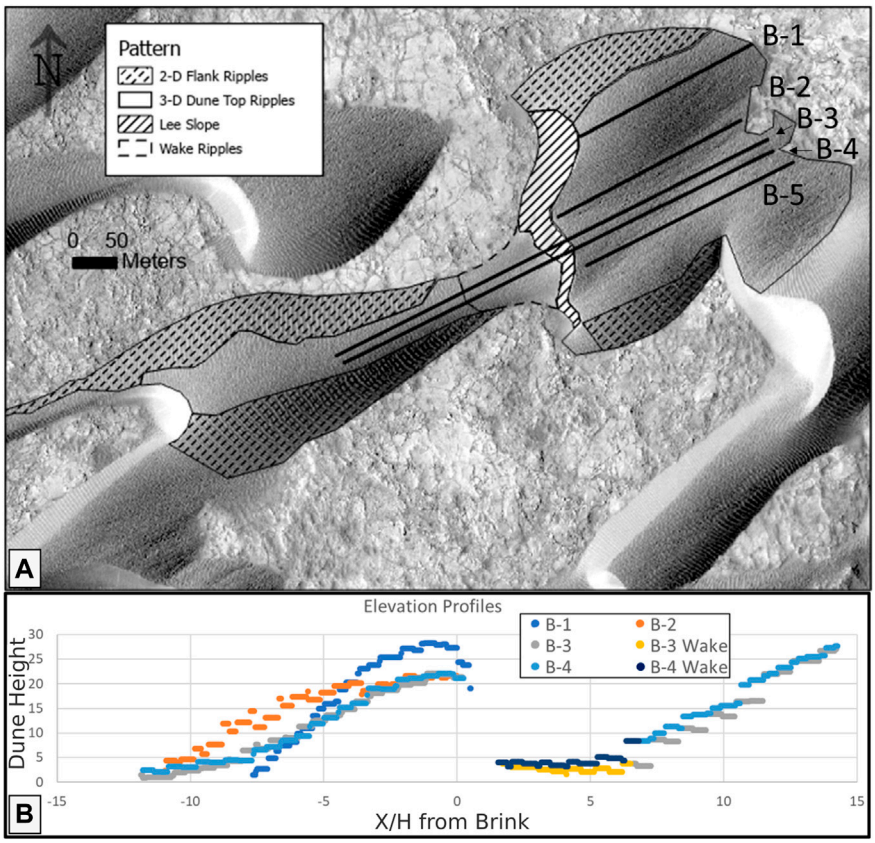

FIGURE 5 | Image of Dune B with ripples and transects mapped. Elevation along each transect is shown in the lower right corner, with lee slopes removed for clarity and areas mapped as "Wake Ripples" highlighted in the profile. The distance from the brink is measured positive in the downwind direction. For clarity, the profile for B-5 is not included as it is nearly identical to the profiles for B-3 and B-4. Artifacts in the elevation data are due to the spline fit used to model the sub-dune bedrock.

ripples occurs at ~5 X/H. In Dune B, wake zones show a rising R/H which peaks and declines after ~6 X/H, aligned with the transition to 3-D ripples. In Dune C, the wake zone shows highly variable R/H, but after the transition to 3-D ripples at 5 X/H both the R/H and variability of R/H drop. Although these patterns are not identical, they collectively indicate a relationship between ripple pattern and ripple migration rate. The wake zones show higher R/H than areas with 3-D ripples thereby defining a distinct zone associated with the dune lee side in which the winds are different from other areas of the dune field. Plots of ripple migration rate vs elevation (**Figure 9**) confirm that the anomalous R/H is not solely due to the low elevation of the wake areas. Dune stoss slopes at the same elevations show the expected linear height-migration rate relationship (e.g., Transect A-2 **Figure 9A**). Though the slope of the linear relationship is often different for each of the dunes in the pair, the wake zones do not plot along these linear trends. Transects A-2, A-3, and B-4 show this contrast clearly and wake zones are apparent as a low-R, low-elevation cluster that is distinct from the linear trend of the dunes.

These analyses show similar patterns among a set of dunes within a single timeframe, but do not address temporal patterns that could be induced by seasonal variations in migration rates linked to changing wind patterns (Ayoub et al., 2014). **Figure 10** shows R/H along transects A-2 and A-3 (**Figure 4**), similar to those shown in **Figure 7**. However, these plots show R/H for different ripple migration maps generated from different pairs of HiRISE images (see **Table 1**) and represent different times of the martian year. Between timesteps, the overall R/H magnitude changes, but pattern of R/H on these stoss slopes is not greatly affected. In both transects, a rise in R/H within the wake reaches a peak at the ripple pattern boundary at 4 – 7 X/H. The location of this peak shifts in different timesteps, though no association between season and peak location is apparent. In two flux maps (032056, Ls = 320–350 and 036091, Ls 114–127, **Table 1**), overall higher R/H exists. In transect A-2 (**Figure 10A**) the peak R/H clearly occurs at ~8 X/H in map 032056, but the peak occurs at ~5 X/H in map 036091 despite both showing above-average R/H in these time periods. It is clear that the activity of these ripples changes throughout the martian year (Ayoub et al., 2014), but these changes in R/H do not lead to changes in the location of peak R/H along the transect indicating this is a robust feature of the dune-modified flows. In addition, when considering the average R/H for all timesteps, the peak R/H occurs close to the mapped wake to 3-D ripple transition (**Figure 10**).

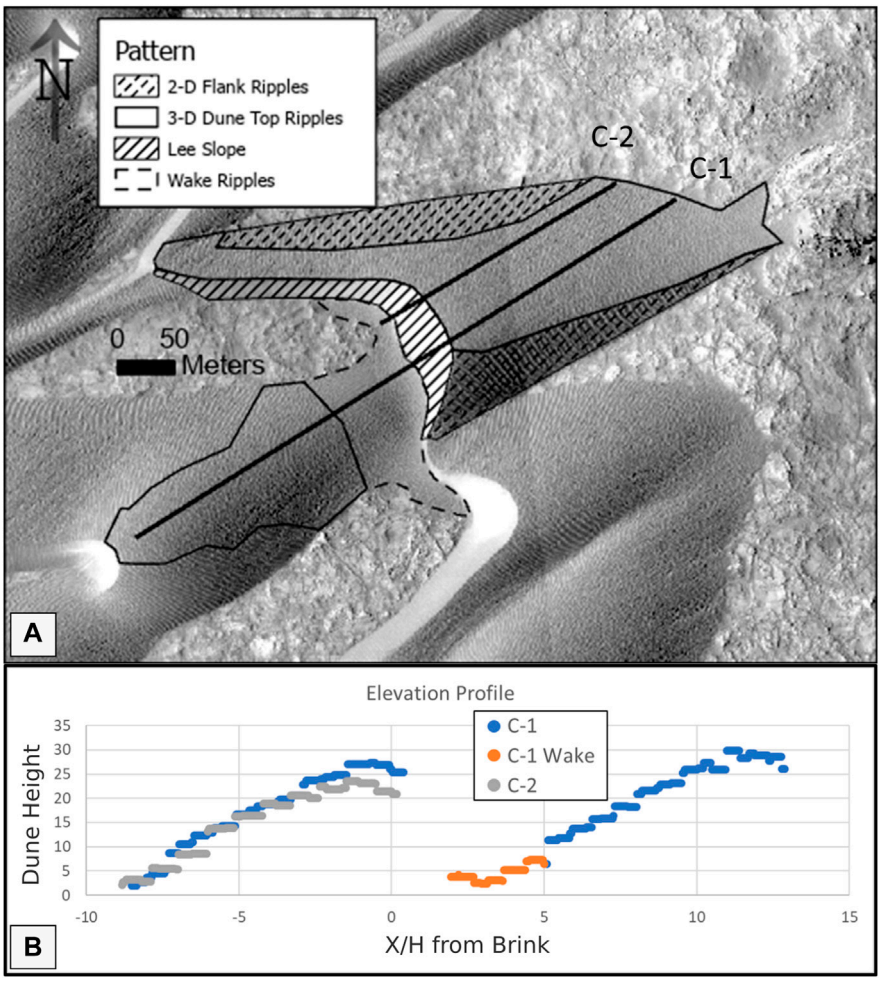

FIGURE 6 | Image of Dune C with ripples and transects mapped. Elevation along each transect is shown in the lower right corner, with lee slopes removed for clarity and areas mapped as "Wake Ripples" highlighted in the profile. The distance from the brink is measured positive in the downwind direction. Artifacts in the elevation data are due to the spline fit used to model the sub-dune bedrock.

Summarily, these observations show that ripple migration rate varies predictably along the dune profile, and that there is an association between the observed ripple migration rates and ripple patterns. Stoss slopes covered in 3-D ripples have a linear relationship between ripple migration rate and height along the dune. This relationship is established within ~5 brink heights on dunes lacking an upwind obstruction, and within 5–10 brink heights of the wake to 3-D ripple transition on trailing dunes. Within wake zones, R/H is higher and reaches a peak near the wake to 3-D ripple pattern boundary. Furthermore, the location of this peak is temporally variable by 1–2 brink heights for an individual dune, but no relationship between peak location and season is apparent.

Wind Orientation

Any regional wind blowing across a dune field results in dune-modified winds due to the influence of the topography of the dunes. We refer to dune-modified flows as "local wind" which may differ from the regional winds. The regional wind is inferred from the COSI-Corr detection of dune top ripple motion, which likely best represents the winds in the vicinity of the dune. Using the Howard (1977) method with measured ripple and slope parameters we determine the formative wind direction for 2-D ripples on slopes. This approach provides an independent indicator of wind direction, which informs how winds may locally deviate from the regional wind. This method requires an estimation of the angle of repose. Multiple values for the angle of repose (α) between 26° and 30°were explored, consistent with findings on Mars (Atwood-Stone and McEwen, 2012; Ewing et al., 2017). With varying angle of repose, the differences in interpreted wind direction are minor (~2°). We use $\alpha = 30°$ for the calculations shown below but use of other angle within the range yielded similar results. Uncertainty in other shape parameters (slope angle, slope orientation) is not explored in detail, but are not expected to exceed ~±2°, and will lead to similar, minor changes in interpreted wind direction as the aforementioned uncertainty in angle of repose.

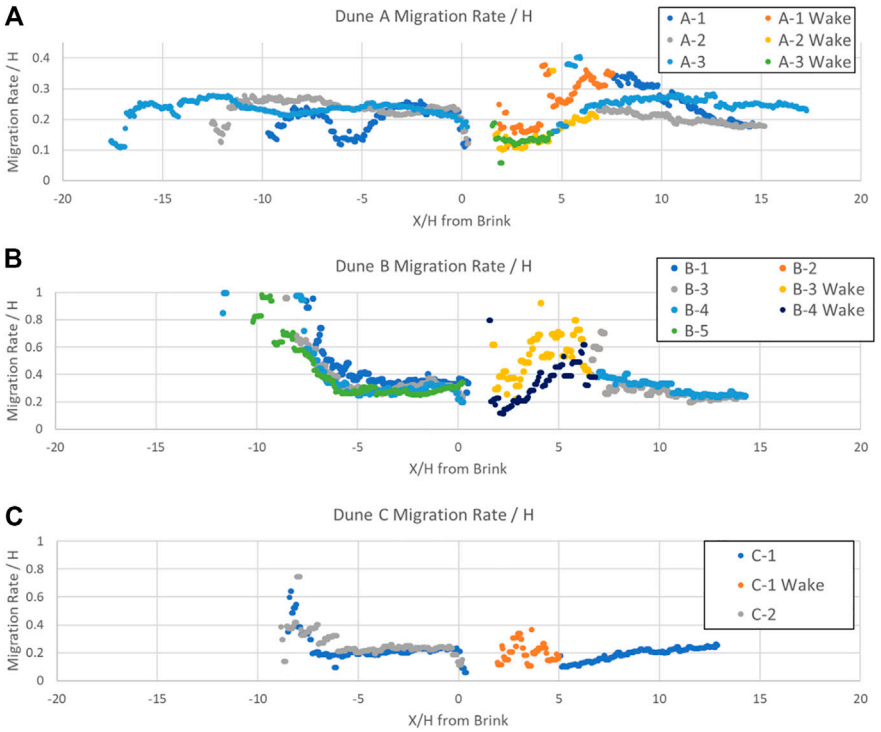

FIGURE 7 | Ripple Migration Rate/H (R/H) for selected transects along Dunes **(A-C)** with areas mapped as wakes highlighted in cases where the transect crosses a wake. Most transects show a similar pattern: Dune stoss slopes reach a constant R/H within 3–4 brink heights of the upwind side of the dune and areas mapped as wake ripples generally deviate from this stoss slope pattern. In Dune **(A)**, the wake zones appear as extended areas of rising R/H, extending between 4 and 7 H from the brink. In Dune **(B,C)**, the wake zones show some ramp up, but also show a higher R/H than the stoss slope of the trailing dune. As shown in **Figures 2**, **3**, the front of the leading dune in dunes B and C falls close to the datum used to calculate dune height, leading to the high R/H values at the front of those dunes.

Site D presented the best opportunity to examine 2-D ripples in the absence of any upwind obstructions. Calculations of the local wind direction were done on 2-D ripples along a 500 m south-facing slope of an extended barchanoid dune arm (**Figure 3**). The regional wind direction determined from 3-D ripples on this dune has an average orientation of 254°. A shift from ~250° at the upwind end to ~263° at the downwind extent of the arm is present. The 2-D ripples along this dune flank begin ~100 m downwind from the main dune and grow to a constant length of ~40 m long. The local wind direction determined from the orientation of 2-D ripples at the upwind end of the slope is ~250° and shifts along slope toward ~268°. Both the dune-top winds and local winds demonstrate a similar, gradual change in wind orientation along the slope. However, local winds on the 2-D ripple bearing slope appear to track these changes more sensitively, changing over a shorter distance and exhibiting a larger overall change (**Figure 3**). This pattern in which local winds shift along with, and sometimes in excess of, regional winds occurs at all other study sites.

The motion of 3-D ripples on the upwind dune at study site E signals a wind direction toward ~256° at the upwind end (**Figure 11**) which gradually shifts to ~270° at the downwind end of the dune. On the eastern slope of the upwind dune (**Figure 11**, Area II), 2-D ripples indicate winds oriented toward ~245° which gradually rotate clockwise toward ~270° at the downwind end. This repeats the pattern seen at site D, where local winds on slopes exposed to regional wind align with the regional wind but show greater variation in orientation. On the western slope of the upwind dune (**Figure 11** Area I), 2-D ripples indicate winds oriented toward the south, ~190°. This is a substantial deviation from the regional winds, though the location of this slope on the western side of the dune may shelter it from regional winds. Similar differences in local and regional wind direction occur on other slopes that are sheltered from the regional winds by upwind dunes. On another dune in study site E (**Figure 11**, Area III), motion of dune-top ripples indicates winds oriented toward ~260°. 2-D ripples along the eastern side indicate similarly oriented winds on the flank without significant change. On the west side of this dune, 2-D ripples indicate winds oriented toward ~200°, repeating the pattern of local wind deviation from regional wind on sheltered slopes as seen in Area I.

The 2-D ripple analysis done at study site F focuses on three dunes that form near the part of the dune field where sand coverage becomes nearly continuous (**Figure 12**). Two elongate dunes form downwind and offset from a central larger dune and have 2-D ripples on their north and south-facing flanks. 3-D ripple motion on the northern dune indicates regional winds oriented toward ~260° and 2-D ripples on the south-facing slope indicate winds oriented toward ~265°. Motion of 3-D ripples on the southern dune-top indicate winds oriented toward ~250° with little change along the dune (**Figure 12**). On the north-facing

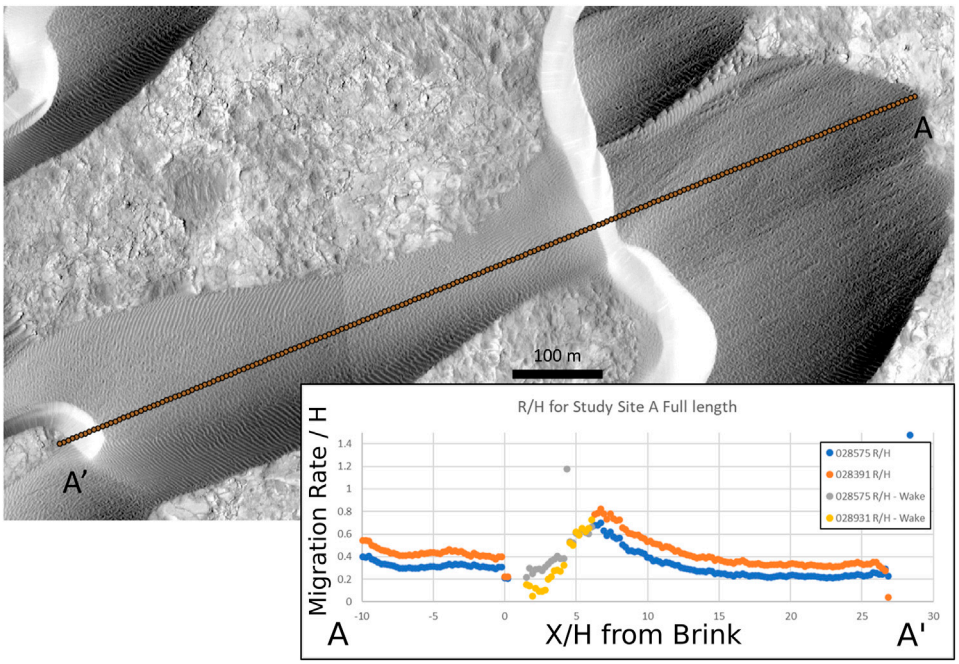

FIGURE 8 | Full transect for Site A. This transect was chosen to explore the R/H along the full length of the second dune, which was not explored in the original data. This transect runs parallel to the morphology of the dune, rather than the wind direction implied from COSI-Corr.

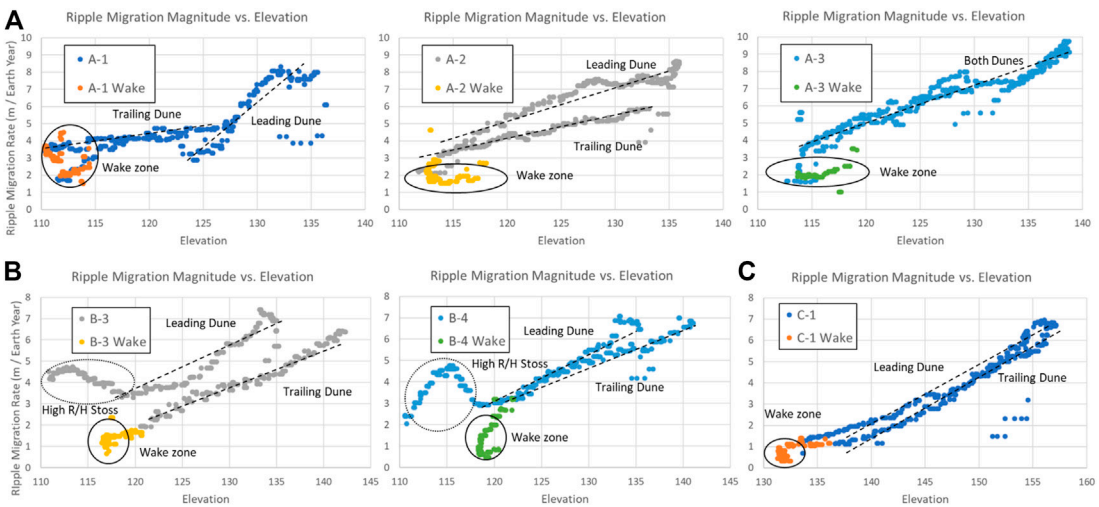

FIGURE 9 | Ripple migration magnitude (R) vs. elevation for selected transects on Dunes **(A-C)**. Elevation is used here instead of dune height to avoid issues arising from either the arbitrary selection of datum or the interpolation of bedrock elevations used to determine dune height in some analyses. These plots show that the wake zones (highlighted in each plot) plot distinctly from the overall linear trend expected for these dunes as highlighted by the dashed lines. In most cases the wakes plot as low-magnitude clusters or follow linear trends offset from the leading and trailing dunes in each dune study area.

flank of the southern dune, ripples initiate on a plinth-like structure beneath the extended lee-slope of the upwind large dune. At this point of incipience, winds indicated by 2-D ripples are oriented toward ~200° (**Figure 12**). As shown in **Figure 12**, winds indicated by 2-D ripples on the northern slope become aligned with dominant winds within 100 m of formation. The south-facing slope of the southern dune is morphologically distinct from the northern slope as it is steeper and has a more abrupt change in slope at the contact with the 3-D ripple bearing dune-top. On the southern slope, winds indicated by 2-D ripples are oriented toward ~285°, showing little change in orientation along the slope. Interestingly, this

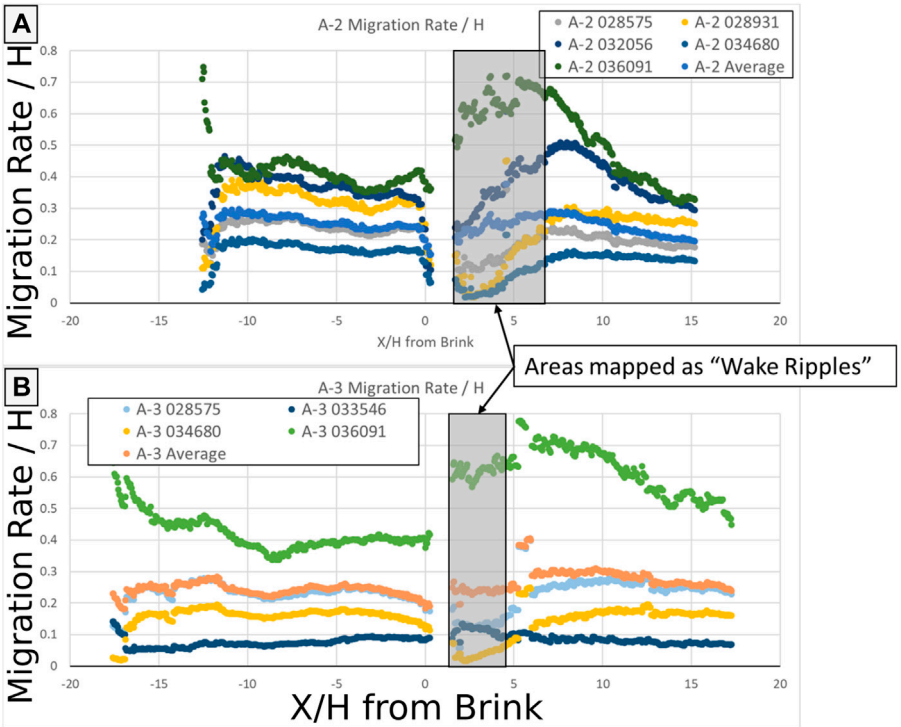

FIGURE 10 | R/H for multiple timesteps for Transects A-2 **(A)** and A-3 **(B)**. The "028575" maps are the data shown in **Figures 6**, **8**, and the other data were chosen as representative of the diversity of lee-wake patterns seen in each case. In both cases, the pattern of R/H in map 028575 was commonly repeated in other maps, although with a variable average R/H.

slope lacks an apparent upwind obstruction that may shelter it from dominant winds as has been observed on other slopes with similar deviations (i.e., **Figure 11**, Area I).

Collectively, these results highlight two common patterns on 2-D ripple bearing slopes. On many slopes, local winds indicated by 2-D ripples deviate from the regional wind near the point of 2-D ripple incipience, but gradually become aligned with the dominant wind. Many slopes that followed this behavior were east-facing and would be exposed to the northeasterly winds that generate the dune field. On other slopes, especially those that may be sheltered from the regional wind, local winds can deviate up to 50° from regional winds and some apparently unsheltered slopes still show notable and consistent deviation. These observations indicate varying degrees of influence of secondary flows on ripple orientation and migration generated in the wakes of upwind dunes.

DISCUSSION

Ripple migration rates and ripple patterns, and local wind direction determined from ripples present a broad set of indicators of airflow over dunes in the Nili Patera dune field. Such observations capture a unique view of airflow across dune topography feasible on Mars due to the large scale of ripples on dunes. By comparison to Earth, these observations also provide new insights to how airflow across dunes might differ due to differences in atmospheric density, which is sixty times lower on Mars. Understanding the behavior of winds on Mars provides a basis to understand planetary aeolian resurfacing (e.g., Golombek et al., 2006; Day and Kocurek, 2018), which has implications for understanding the age and exposure history of surface materials that could affect the preservation potential of ancient life (Day and Anderson, 2021). Observations that inform the modern aeolian environment and the processes within it serve as an important connection to paleo-environments on Mars. Furthermore, near-surface winds present a serious hazard for surface exploration, both robotic and human. Improving our understanding of flow-topography interactions will help to better predict surface winds at finer resolution and increase the safety of landing in areas where surface winds are strongly influenced by local topography.

Measurement of Reattachment Length

Recognized from exhaustive studies of air and water flow over dunes, two major components of airflow in a dune wake are the point of airflow separation (where the internal boundary layer becomes detached from the dune surface) and the zone of reattachment (where the boundary layer re-attaches to the dune surface). The point of separation is typically taken to occur at the dune brink, and the area between this and the reattachment zone is where secondary airflow dominates. Reversed airflow and along-dune vortices exist in this zone, and wind velocities are generally lower (e.g., Walker and

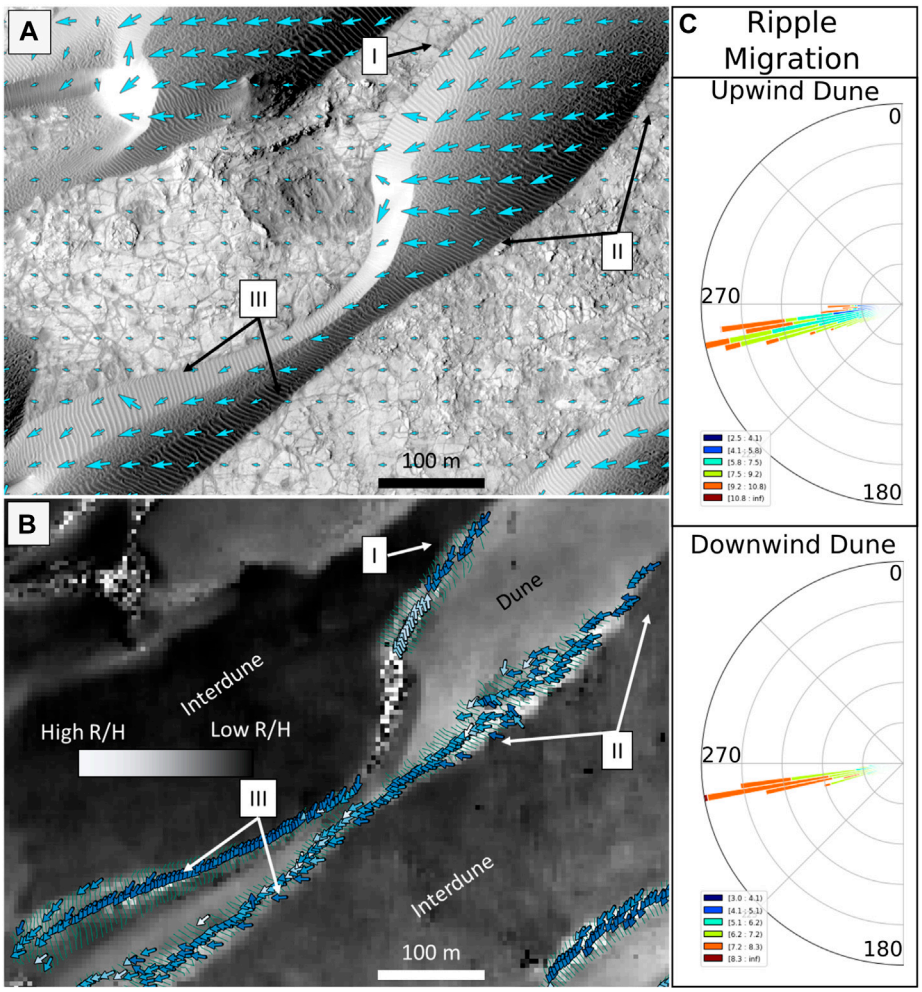

FIGURE 11 | Imagery and ripple migration directions **(A)** and Ripple migration rate over dune height **(B)** maps of site E with **(C)** rose diagrams of ripple migration direction and magnitude for each dune top. Site E captures a number of features that are commonly seen on these steep, ripple bearing slopes. Roman numerals and arrows indicate three 2-D ripples bearing slopes that demonstrate several observed behaviors.

Nickling, 2003; Dong et al., 2009; Baddock et al., 2011). The linear ripple-migration rate to dune height relationship, which originates from streamline compression (Bridges et al., 2012), should also break down in the reattachment zone. We interpret the deviated R/H patterns observed in wake zones, as well as the associated ripple patterns, to denote this zone of reversed flow on martian dunes. In these dune pairs, R/H rises sharply within the wake zones and decreases at the wake-zone to 3-D ripple pattern boundary (**Figure 7**). After this transition, the pattern in R/H is similar to the pattern seen at leading dune toes; a decline in R/H which reaches a stable value 5–10 brink heights from the wake to 3-D transition. This sharp transition is interpreted as the line of attachment in which return flow moves toward the slipface and attached flow is re-established downwind of the line. This pattern is most clearly represented in transects A-1, A-2, B-3, and B-4 (**Figures 7A,B**).

Variance in wake-zone behavior is evident among the dunes analyzed and may be related to differences in dune morphology and upwind settings. Transect A-3 (**Figure 7A**) shows a low R/H within the wake zone and no peak in R/H at the wake to 3-D ripple pattern boundary. This lack of reattachment zone definition may be related to the difference in crest-brink separation on the leading stoss slope. A-3 has greater crest brink separation than transects A-1 and A-2 which, according to measurements from Earth, would decrease the flow reattachment length (Baddock et al., 2011) consistent with the observations here. **Figure 9** shows that, despite the high R/H, the mapped wake zones show the lowest ripple migration rates within the analyzed transects, consistent with low wind speed expected in this zone. Furthermore, **Figure 10** shows that the pattern of R/H across the ripple pattern transition is relatively consistent over time for a given dune. This consistency suggests that the variance in R/H pattern among the study sites is related to features of the dunes themselves (i.e., dune shape, position in the dune field, relative location to other dunes, etc.). The low ripple migration rates and deviation from the linear R/H

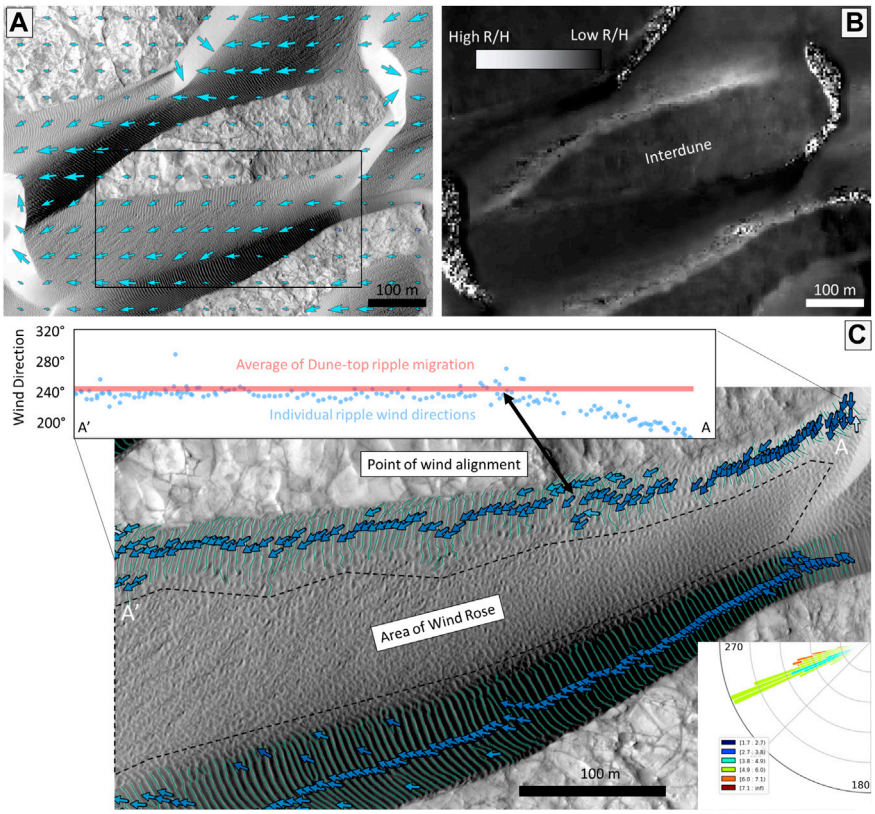

FIGURE 12 | Imagery and ripple migration directions **(A)** and ripple migration rate over dune height **(B)** maps of site F. **(C)** Closer examination of the southern dune. The rose diagram indicates the direction of ripple motion within the outlined area, showing little change over the dune top. Local winds on the north-facing slope show initial deviation, then alignment with the regional wind at the location indicated by the black arrow. On the southern slope, local winds show consistent deviation from the regional wind along the slope.

relationship, are consistent with the distinct boxwork ripple patterns which highlight the complexity of wind flows affecting the ripples in this area of the dune. Flow 2-D and 3-D turbulent recirculation cells with high turbulent kinetic energy could impart varying flow directions that would give rise to the complex ripple patterns (Walker and Nickling, 2003; Dong et al., 2009; Wang and Anderson, 2019). Collectively, these observations suggest that the mapped wake zones, which bear both ripple patterns and ripple migration rates distinct from other dune areas, coincide with zones of reversed flow.

The boundaries of the recirculation zone determined by the R/H and ripple patterns can be used to measure the reattachment length of airflow across martian dunes. Previous terrestrial work sought to determine characteristic lengths of reattachment based on both the height of the dune and the degree of separation between the dune crest and brink (Baddock et al., 2011). Two dune shapes, crest-brink coincident (CBC) and crest-brink separated (CBS), were found by Baddock et al. (2011) to have reattachment lengths of 6.5–8.6 brink heights and 2–5 brink heights respectively. While these constraints are broad, they set the general expectation that closer spacing of the crest and brink will lead to longer reattachment lengths due to the abrupt change in topography. Using the boundary of mapped wake ripples as the zone where flow becomes reattached, measurements of reattachment lengths on the Nili Patera dunes fell between 4 and 7 brink heights (**Figure 7**). This consistency of reattachment lengths between Earth and Mars is theoretically reasonable, as it has been shown that turbulent (high-Reynolds number) flows are scale-invariant (Meneveau and Katz, 2000) and turbulent flow models have worked well in studies of the martian surface (Day and Anderson, 2021; Runyon et al., 2017). This scale invariance also explains why temporal changes in apparent reattachment lengths (peak R/H values, **Figure 10**) do not scale with overall migration magnitude. These changes are likely due to seasonal changes in regional wind direction which lead to differing secondary flow development in the dune wake. Seasonally variable wind directions are likely given the asymmetric shape of many dunes in this field (e.g., Site D, **Figure 2**), though dune shapes are also influenced by interactions and local topography (Bourke, 2010; Parteli et al., 2014). Furthermore, terrestrial reattachment lengths (Baddock et al., 2011) were measured on isolated dunes, where dunes within a dune field are expected to have ~25% shorter reattachment lengths (Schatz and Herrmann, 2006). Given that these observations are measured on dune pairs and are likely subject to this shortening effect, it may be reasonable to estimate that an isolated martian dune would have a reattachment length of up to 8-9 brink heights.

Wind Orientation on Steep Slopes

Measurement of formative wind directions along 2-D ripple bearing slopes provides insight into how upwind dunes modify airflow that affects downwind dunes and the processes responsible for 2-D ripple formation. The ripples on these slopes indicate that the local winds are either aligned with regional winds determined from dune-top ripples or deviated significantly from regional winds. Slopes on which local winds were aligned to the regional wind were typically east-facing and transitioned along low slopes to neighboring 3-D ripple-bearing terrain. Examples of such slopes can be found at sites D and E, where local winds align with the regional winds (**Figures 3**, **11**). However, in most of these cases, along-slope variations in local wind are apparent. Both regional winds and local winds showed evidence for rotation along the dune, for example in site D where both local and regional winds shift in a clockwise direction. However, local winds track this change more sensitively than the regional winds, generally showing a larger change in direction over the length of the dune (e.g., sites D and E). These patterns appear in the absence of any immediate upwind obstructions that may shelter or substantially deflect wind. We interpret this to demonstrate the portion of the regional flow that is deflected around the dune rather than over the dune. The gradual shift in local winds may indicate that deflected winds become less significant as you move downwind on a single slope. If flow is notably deflected around dunes, this may suggest that these 2-D ripple slopes act as significant channels for sediment. Ripple migration rates on these slopes do not generally exceed migration rates on dune-tops, but these slopes show a high R/H relative to nearby slopes lacking 2-D ripples (**Figures 11**, **12**).

The second group of 2-D ripple bearing slopes were those with local winds strongly deviated from the regional wind. In some cases, such as in Site E (**Figure 11** Area I, III), slopes are north or west-facing and might be predicted to be sheltered from the regional wind which is oriented toward the southwest. Sheltering from regional winds could prevent these ripples from being reworked during the most frequent wind events, allowing them to record a secondary, oblique wind mode from which it is not sheltered. Another possibility is that these ripples are formed during the same wind events that generate dune-top winds and arise from dune-flow interactions. In the latter explanation these slopes indicate substantial, sand-moving winds forming in some flow separation cells. Predictably, these north-facing slopes with 2-D ripples, as well as those in immediate dune wakes, do not show such a high R/H. Ripples on these slopes are more likely formed by some combination of lesser wind modes and secondary flows that arise from dune topography with either weaker or more intermittent flow.

The southernmost ripple-bearing slope of Site F (**Figure 12C**) presents an interesting example in which local winds are deviated from regional winds. As discussed in *Wind Orientation*, this slope shows local winds (oriented toward ~280°) that consistently deviate from the regional winds (oriented toward 250°) along the entire slope, but there is no apparent obstruction sheltering the slope from regional winds. This lack of apparent sheltering suggests that the local wind on this slope is coincident with the regional wind events and arises from complex dune-flow interaction. Wind on this slope is likely the combined effect of flow channeling from upwind dunes to the ENE and flow diversion from a dune to the SE (**Figure 2**). The orientation of this local wind suggests vortex development rotating counterclockwise (from the overall SW-oriented regional wind). Experimental observation of interacting barchan dunes suggests that vortex development on a slope in this interaction environment should rotate in the opposite (i.e., clockwise) direction (Bristow, et al., 2020, **Figure 10**). The experimental approach only considers two interacting barchans, a smaller one upstream and offset of a larger one, which may approximately simulate the two dunes upwind of the slope of interest. The third dune, toward the SE and only partially upwind of the slope, may therefore be an important aspect in generating the inferred vortex rotating in the opposite sense than predicted.

Notably, the 2-D ripple bearing slopes formed almost exclusively on slopes >~20°. The methodology applied above assumes that the slope effect is the primary reason for ripples to form oblique to wind direction (e.g., Rubin, 2012), and the exclusivity of 2-D ripple formation to steeper slopes supports this assumption. Bi-directional winds are also a known cause of ripple straightening (Rubin, 2012), and may play a role in the formation of these ripples especially where they form on lower slopes or in dune wakes. For the first class of 2-D ripples discussed above (slopes exposed to the regional wind), **Eq. 1** provides realistic results that likely capture the primary influences on 2-D ripple formation. However, for the slopes sheltered from the regional wind (e.g., Site E area I, **Figure 11**) the potential for secondary winds is greater. In such areas, the interaction of multiple wind modes may be responsible for 2-D ripple formation, which is more easily recorded due to sheltering from the dominant regional wind. However, even in these areas the slope-induced component is likely significant if the slope approaches ~20°. Consideration of the combined effect of multi-directional winds in addition to slope-induced obliquity could be fruitful on these steep sheltered slopes and is a topic for future work. Whether the winds inferred on sheltered slopes are due to dune-flow interaction, secondary wind modes, or non-unidirectional wind regimes, these observations provide evidence of complex flow occurring in the modern martian aeolian environment.

CONCLUSION

To examine airflow over a dune, through the dune lee side, and onto the downwind dune, we make observations of ripple migration over select upwind-downwind dune pairs (*Ripple Migration Rates on Dunes*) with continuous sand coverage (i.e., no exposed bedrock). Key measurements arising from this are measurements of flow reattachment in the wake zone of a dune and flow recovery lengths to the dominant wind. We also examine how the dominant, regional airflow is deflected by dune topography by measuring 2-D ripples that exist on dune flanks (*Wind Orientation*). We find two types of slopes that exhibit 2-D ripples, one exposed to regional winds and another more influenced by oblique secondary winds. These ripples, particularly those recording secondary winds, are useful detectors of local

flow and demonstrate areas of flow separation, and potentially significant vortex development.

Observations of ripple migration rates and ripple patterns provide a method to determine reattachment lengths on martian dunes, but many details of the controls on reattachment zone shape are still unclear. Among the dunes measured, there is no apparent relationship between crest-brink separation distance and reattachment length as seen on Earth (Baddock et al., 2011), though there is a lack of sampling diversity as most transects show a close crest-brink spacing. More widespread analysis may provide sufficient observations to demonstrate such a correlation between crest-brink spacing and reattachment length on Mars and determine how these relationships may change in other dune fields. Analysis of 2-D ripples demonstrates direct evidence for oblique wind flow in the wake of martian dunes, but it is not clear whether the flows recorded by these ripples are temporally coincident with the wind events that generate ripple motion on the dune tops. If a secondary regional wind mode sufficient to create 2-D ripples on these sheltered slopes is present, this could explain observed dune asymmetries within the Nili Patera dune field (Bourke, 2010) though this field is expected to arise from a unidirectional wind regime (Chojnacki et al., 2019). Some 2-D ripples (e.g., study site F) are not sheltered from regional winds and are therefore generated by secondary winds and vortices that develop coincident to the regional wind events (*Wind Orientation on Steep Slopes*). This supports the notion that dune-steered flows and secondary regimes are strong enough to mobilize sand on Mars (Jackson et al., 2015).

These findings further demonstrate the utility of ripple-tracking techniques, and their combination with independent estimates of flow direction provides further detail on flow-topography interaction. These observations provide new estimates of reattachment lengths on Mars, a key feature in understanding complex wake zone flow dynamics. The connection between ripple patterns and ripple migration is particularly useful, as this allows examination of dune wake zones where data is lacking to carry out high-resolution ripple tracking.

DATA AVAILABILITY STATEMENT

The original contributions presented in the study are included in the Mendeley Data Repository: 10.17632/xk479zkpm8.1, further inquiries can be directed to the corresponding author.

AUTHOR CONTRIBUTIONS

DH was primarily responsible for writing the manuscript and was the primary researcher on the project. RE advised DH in the writing and research process. KR generated the COSI-Corr data used in the analysis. KR provided revisions on the manuscript and provided scientific guidance to the project. J-PA provided revisions on the manuscript and provided guidance on the application of the COSI-Corr methodology. MM aided in ripple tracing, providing data to the analysis.

FUNDING

This work was funded primarily by the Mars Data Analysis Program (Grant #NNX16AJ43G).

REFERENCES

Assis, W. R., and Franklin, E. D. M. (2020). A Comprehensive Picture for Binary Interactions of Subaqueous Barchans. *Geophys. Res. Lett.* 47 (18), e2020GL089464. doi:10.1029/2020gl089464

Atwood-Stone, C., and McEwen, A. S. (2013). Avalanche Slope Angles in Low-gravity Environments from Active Martian Sand Dunes. *Geophys. Res. Lett.* 40 (12), 2929–2934. doi:10.1002/grl.50586

Ayoub, F., Avouac, J.-P., Newman, C. E., Richardson, M. I., Lucas, A., Leprince, S., et al. (2014). Threshold for Sand Mobility on Mars Calibrated from Seasonal Variations of Sand Flux. *Nat. Commun.* 5, 1–8. doi:10.1038/ncomms6096

Bacik, K. A., Lovett, S., Colm-cille, P. C., and Vriend, N. M. (2020). Wake Induced Long Range Repulsion of Aqueous Dunes. *Phys. Rev. Lett.* 124 (5), 054501. doi:10.1103/physrevlett.124.054501

Baddock, M. C., Wiggs, G. F. S., and Livingstone, I. (2011). A Field Study of Mean and Turbulent Flow Characteristics Upwind, over and Downwind of Barchan Dunes. *Earth Surf. Process. Landforms* 36 (11), 1435–1448. doi:10.1002/esp.2161

Bagnold, R. A. (1941). *The Physics of Blown Sand and Desert Dunes*. London: Chapman & Hall.

Bennett, S. J., and Best, J. L. (1995). Mean Flow and Turbulence Structure over Fixed, Two-Dimensional Dunes: Implications for Sediment Transport and Bedform Stability. *Sedimentology* 42 (3), 491–513. doi:10.1111/j.1365-3091.1995.tb00386.x

Bourke, M. C. (2010). Barchan Dune Asymmetry: Observations from Mars and Earth. *Icarus* 205 (1), 183–197. doi:10.1016/j.icarus.2009.08.023

Bridges, N. T., Ayoub, F., Avouac, J.-P., Leprince, S., Lucas, A., and Mattson, S. (2012). Earth-like Sand Fluxes on Mars. *Nature* 485 (7398), 339–342. doi:10.1038/nature11022

Bridges, N. T., Geissler, P. E., McEwen, A. S., Thomson, B. J., Chuang, F. C., Herkenhoff, K. E., et al. (2007). Windy Mars: A Dynamic Planet as Seen by the HiRISE Camera. *Geophys. Res. Lett.* 34 (23). doi:10.1029/2007GL031445

Bristow, N. R., Blois, G., Best, J. L., and Christensen, K. T. (2020). Secondary Flows and Vortex Structure Associated with Isolated and Interacting Barchan Dunes. *J. Geophys. Res. Earth Surf.* 125 (2), 1–30. doi:10.1029/2019JF005257

Bristow, N. R., Blois, G., Best, J. L., and Christensen, K. T. (2019). Spatial Scales of Turbulent Flow Structures Associated with Interacting Barchan Dunes. *J. Geophys. Res. Earth Surf.* 124 (5), 1175–1200. doi:10.1029/2018JF004981

Bristow, N. R., Blois, G., Best, J. L., and Christensen, K. T. (2018). Turbulent Flow Structure Associated with Collision between Laterally Offset, Fixed-Bed Barchan Dunes. *J. Geophys. Res. Earth Surf.* 123 (9), 2157–2188. doi:10.1029/2017JF004553

Chojnacki, M., Banks, M. E., Fenton, L. K., and Urso, A. C. (2019). Boundary Condition Controls on the High-Sand-Flux Regions of Mars. *Geology* 47 (5), 427–430. doi:10.1130/G45793.1

Chojnacki, M., Burr, D. M., Moersch, J. E., and Michaels, T. I. (2011). Orbital Observations of Contemporary Dune Activity in Endeavor Crater, Meridiani Planum, Mars. *J. Geophys. Res. Planets* 116 (E7). doi:10.1029/2010je003675

Claudin, P., Wiggs, G. F. S., and Andreotti, B. (2013). Field Evidence for the Upwind Velocity Shift at the Crest of Low Dunes. *Boundary-layer Meteorol.* 148 (1), 195–206. doi:10.1007/s10546-013-9804-3

Cooper, W. S. (1958). Coastal Sand Dunes of Oregon and Washington. *Memoir Geol. Soc. America* 72 (1), 1–162. doi:10.1130/MEM72-p1

Courrech du Pont, S., Narteau, C., and Gao, X. (2014). Two Modes for Dune Orientation. *Geology* 42 (9), 743–746. doi:10.1130/G35657.1

Day, M., and Anderson, W. (2021). Wind Erosion on Mars Exposes Ideal Targets for Sample Return. *Geophys. Res. Lett.* 48 (2), 1–10. doi:10.1029/2020GL090580

Day, M., and Kocurek, G. (2018). Pattern Similarity across Planetary Dune fields. *Geology* 46 (11), 999–1002. doi:10.1130/G45547.1

Dong, Z., Qinan, G., Lu, P., Luo, W., and Wang, H. (2009). Turbulence fields in the lee of Two-Dimensional Transverese Dunes Simulated a Wind Tunnel. *Earth Surf. Process. Landforms* 34 (March), 613–628. doi:10.1002/esp.1704

Eastwood, E. N., Kocurek, G., Mohrig, D., and Swanson, T. (2012). Methodology for Reconstructing Wind Direction, Wind Speed and Duration of Wind Events from Aeolian Cross-Strata. *J. Geophys. Res.* 117 (3), a–n. doi:10.1029/2012JF002368

Ewing, R. C., and Kocurek, G. (2010). Aeolian Dune-Field Pattern Boundary Conditions. *Geomorphology* 114 (3), 175–187. doi:10.1016/j.geomorph.2009.06.015

Ewing, R. C., Lapotre, M. G. A., Lewis, K. W., Day, M., Stein, N., Rubin, D. M., et al. (2017). Sedimentary Processes of the Bagnold Dunes: Implications for the Eolian Rock Record of Mars. *J. Geophys. Res. Planets* 122 (12), 2544–2573. doi:10.1002/2017JE005324

Ewing, R. C., Peyret, A. P. B., Kocurek, G., and Bourke, M. (2010). Dune Field Pattern Formation and Recent Transporting Winds in the Olympia Undae Dune Field, north Polar Region of Mars. *J. Geophys. Res. Planets* 115 (E8). doi:10.1029/2009je003526

Frank, A., and Kocurek, G. (1996a). Toward a Model for Airflow on the lee Side of Aeolian Dunes. *Sedimentology* 43 (3), 451–458. doi:10.1046/j.1365-3091.1996.d01-20.x

Frank, A. J., and Kocurek, G. (1996b). Airflow up the Stoss Slope of Sand Dunes: Limitations of Current Understanding. *Geomorphology* 17 (1-3), 47–54. doi:10.1016/0169-555x(95)00094-l

Golombek, M. P., Grant, J. A., Crumpler, L. S., Greeley, R., Arvidson, R. E., Bell, J. F., et al. (2006). Erosion Rates at the Mars Exploration Rover landing Sites and Long-Term Climate Change on Mars. *J. Geophys. Res.* 111 (12). doi:10.1029/2006JE002754

Howard, A. D. (1977). Effect of Slope on the Threshold of Motion and its Application to Orientation of Wind Ripples. *Geol. Soc. America Bull.* 88 (6), 853–856. doi:10.1130/0016-7606(1977)88<853:eosott>2.0.co;2

Jackson, D. W. T., Bourke, M. C., and Smyth, T. A. G. (2015). The Dune Effect on Sand-Transporting Winds on Mars. *Nat. Commun.* 6, 1–5. doi:10.1038/ncomms9796

Jackson, P. S., and Hunt, J. C. R. (1975). Turbulent Wind Flow over a Low hill. *Q.J R. Met. Soc.* 101 (430), 929–955. doi:10.1002/qj.49710143015

Jia, P., Andreotti, B., and Claudin, P. (2017). Giant Ripples on Comet 67P/Churyumov–Gerasimenko Sculpted by sunset thermal Wind. *Proc. Natl. Acad. Sci.* 114 (10), 2509–2514. doi:10.1073/pnas.1612176114

Kocurek, G., Carr, M., Ewing, R., Havholm, K. G., Nagar, Y. C., and Singhvi, A. K. (2007). White Sands Dune Field, New Mexico: Age, Dune Dynamics and Recent Accumulations. *Sediment. Geol.* 197 (3–4), 313–331. doi:10.1016/j.sedgeo.2006.10.006

Kocurek, G., Ewing, R. C., and Mohrig, D. (2010). How Do Bedform Patterns Arise? New Views on the Role of Bedform Interactions within a Set of Boundary Conditions. *Earth Surf. Process. Landforms* 35, 51–63. doi:10.1002/esp.1913

Lancaster, N. (1985). Variations in Wind Velocity and Sand Transport on the Windward Flanks of Desert Sand Dunes. *Sedimentology* 32 (4), 581–593. doi:10.1111/j.1365-3091.1985.tb00472.x

Lapôtre, M. G. A., Ewing, R. C., and Lamb, M. P. (2021). An Evolving Understanding of Enigmatic Large Ripples on Mars. *J. Geophys. Res. Planets* 126 (2), e2020JE006729. doi:10.1029/2020je006729

Lapotre, M. G. A., Ewing, R. C., Lamb, M. P., Fischer, W. W., Grotzinger, J. P., Rubin, D. M., et al. (2016). Large Wind Ripples on Mars: A Record of Atmospheric Evolution. *Science* 353 (6294), 55–58. doi:10.1126/science.aaf3206

Lapotre, M. G. A., Ewing, R. C., Weitz, C. M., Lewis, K. W., Lamb, M. P., Ehlmann, B. L., et al. (2018). Morphologic Diversity of Martian Ripples: Implications for Large-Ripple Formation. *Geophys. Res. Lett.* 45 (19), 10,229–10,239. doi:10.1029/2018GL079029

Lee, D. B., Ferdowsi, B., and Jerolmack, D. J. (2019). The Imprint of Vegetation on Desert Dune Dynamics. *Geophys. Res. Lett.* 46 (21), 12041–12048. doi:10.1029/2019GL084177

Leprince, S., Barbot, S., Ayoub, F., and Avouac, J. P. (2007). Automatic and Precise Orthorectification, Coregistration, and Subpixel Correlation of Satellite Images, Application to Ground Deformation Measurements. *IEEE Trans. Geosci. Remote Sensing* 45, 1529–1558. doi:10.1109/tgrs.2006.888937

Liu, Z. Y. C., and Zimbelman, J. R. (2015). Recent Near-Surface Wind Directions Inferred from Mapping Sand Ripples on Martian Dunes. *Icarus* 261, 169–181. doi:10.1016/j.icarus.2015.08.022

Lorenz, R. D. (2020). Martian Ripples Making a Splash. *J. Geophys. Res. Planets* 125 (10), 12–15. doi:10.1029/2020JE006658

Lorenz, R. D., Wall, S., Radebaugh, J., Boubin, G., Reffet, E., Janssen, M., et al. (2006). The Sand Seas of Titan: Cassini RADAR Observations of Longitudinal Dunes. *Science* 312 (5774), 724–727. doi:10.1126/science.1123257

Lucas, A., Narteau, C., Rodriguez, S., Rozier, O., Callot, Y., Garcia, A., et al. (2015). Sediment Flux from the Morphodynamics of Elongating Linear Dunes. *Geology* 43 (11), 1027–1030. doi:10.1130/G37101.1

McEwen, A. S., Eliason, E. M., Bergstrom, J. W., Bridges, N. T., Delamere, W. A., Grant, J. A., et al. (2007). MRO's High Resolution Imaging Science Experiment (HiRISE). *J. Geophys. Res.* 112. doi:10.1029/2005JE002605

Meneveau, C., and Katz, J. (2000). Scale Invariance and Turbulence Models for Large-Eddy Simulation. *Annu. Rev. Fluid Mech.* 32 (1), 1–32. doi:10.1146/annurev.fluid.32.1.1

Neuman, C. M., Lancaster, N., and Nickling, W. G. (1997). Relations between Dune Morphology, Air Flow, and Sediment Flux on Reversing Dunes, Silver Peak, Nevada. *Sedimentology* 44 (6), 1103–1111. doi:10.1046/j.1365-3091.1997.d01-61.x

Newman, C. E., Gómez-Elvira, J., Marin, M., Navarro, S., Torres, J., Richardson, M. I., et al. (2017). Winds Measured by the Rover Environmental Monitoring Station (REMS) during the Mars Science Laboratory (MSL) Rover's Bagnold Dunes Campaign and Comparison with Numerical Modeling Using MarsWRF. *Icarus* 291 (December 2016), 203–231. doi:10.1016/j.icarus.2016.12.016

Parsons, D. R., Walker, I. J., and Wiggs, G. F. (2004). Numerical Modelling of Flow Structures over Idealized Transverse Aeolian Dunes of Varying Geometry. *Geomorphology* 59 (1-4), 149–164. doi:10.1016/j.geomorph.2003.09.012

Parteli, E. J. R., Durán, O., Bourke, M. C., Tsoar, H., Pöschel, T., and Herrmann, H. (2014). Origins of Barchan Dune Asymmetry: Insights from Numerical Simulations. *Aeolian Res.* 12, 121–133. doi:10.1016/j.aeolia.2013.12.002

Roback, K. P., Runyon, K. D., and Avouac, J. P. (2020). Craters as Sand Traps: Dynamics, History, and Morphology of Modern Sand Transport in an Active Martian Dune Field. *Icarus* 342, 113642. doi:10.1016/j.icarus.2020.113642

Rubin, D. M. (2012). A Unifying Model for Planform Straightness of Ripples and Dunes in Air and Water. *Earth-Science Rev.* 113 (3–4), 176–185. doi:10.1016/j.earscirev.2012.03.010

Runyon, K. D., Bridges, N. T., Ayoub, F., Newman, C. E., and Quade, J. J. (2017). An Integrated Model for Dune Morphology and Sand Fluxes on Mars. *Earth Planet. Sci. Lett.* 457, 204–212. doi:10.1016/j.epsl.2016.09.054

Schatz, V., and Herrmann, H. J. (2006). Flow Separation in the lee Side of Transverse Dunes: A Numerical Investigation. *Geomorphology* 81 (1–2), 207–216. doi:10.1016/j.geomorph.2006.04.009

Schatz, V., Tsoar, H., Edgett, K. S., Parteli, E. J., and Herrmann, H. J. (2006). Evidence for Indurated Sand Dunes in the Martian north Polar Region. *J. Geophys. Res. Planets* 111 (E4). doi:10.1029/2005je002514

Silvestro, S., Fenton, L. K., Vaz, D. A., Bridges, N. T., and Ori, G. G. (2010). Ripple Migration and Dune Activity on Mars: Evidence for Dynamic Wind Processes. *Geophys. Res. Lett.* 37 (20). doi:10.1029/2010gl044743

Silvestro, S., Vaz, D. A., Yizhaq, H., and Esposito, F. (2016). Dune-like Dynamic of Martian Aeolian Large Ripples. *Geophys. Res. Lett.* 43 (16), 8384–8389. doi:10.1002/2016GL070014

Smith, A. B., Jackson, D. W., and Cooper, J. A. G. (2017). Three-dimensional Airflow and Sediment Transport Patterns over Barchan Dunes. *Geomorphology* 278, 28–42. doi:10.1016/j.geomorph.2016.10.025

Sullivan, R., Kok, J. F., Katra, I., and Yizhaq, H. (2020). A Broad Continuum of Aeolian Impact Ripple Morphologies on Mars Is Enabled by Low Wind Dynamic Pressures. *J. Geophys. Res. Planets* 125 (10), 1–39. doi:10.1029/2020JE006485

Swanson, T., Mohrig, D., and Kocurek, G. (2016). Aeolian Dune Sediment Flux Variability over an Annual Cycle of Wind. *Sedimentology* 63 (6), 1753–1764. doi:10.1111/sed.12287

Swanson, T., Mohrig, D., Kocurek, G., Perillo, M., and Venditti, J. (2018). Bedform Spurs: a Result of a Trailing Helical Vortex Wake. *Sedimentology* 65 (1), 191–208. doi:10.1111/sed.12383

Telfer, M. W., Parteli, J. R., Radebaugh, J., Beyer, R. A., Bertrand, T., Forget, F., et al. (2018). Dunes on Pluto. *Science* 360 (6392), 992–997. doi:10.1126/science.aao2975

Vaz, D. A., Silvestro, S., Sarmento, P. T. K., and Cardinale, M. (2017). Migrating Meter-Scale Bedforms on Martian Dark Dunes: Are Terrestrial Aeolian Ripples Good Analogues? *Aeolian Res.* 26, 101–116. doi:10.1016/j.aeolia.2016.08.003

Vinent, O. D., Andreotti, B., Claudin, P., and Winter, C. (2019). A Unified Model of Ripples and Dunes in Water and Planetary Environments. *Nat. Geosci.* 12 (5), 345–350. doi:10.1038/s41561-019-0336-4

Walker, I. J., and Nickling, W. G. (2002). Dynamics of Secondary Airflow and Sediment Transport over and in the lee of Transverse Dunes. *Prog. Phys. Geogr.* 26 (1), 47–75. doi:10.1191/0309133302pp325ra

Walker, I. J., and Nickling, W. G. (2003). Simulation and Measurement of Surface Shear Stress over Isolated and Closely Spaced Transverse Dunes in a Wind Tunnel. *Earth Surf. Process. Landforms* 28 (10), 1111–1124. doi:10.1002/esp.520

Wang, C., and Anderson, W. (2019). Turbulence Coherence within Canonical and Realistic Aeolian Dune-Field Roughness Sublayers. *Boundary-Layer Meteorol.* 173 (3), 409–434. doi:10.1007/s10546-019-00477-w

Weitz, C. M., Sullivan, R. J., Lapotre, M. G. A., Rowland, S. K., Grant, J. A., Baker, M., et al. (2018). Sand Grain Sizes and Shapes in Eolian Bedforms at Gale Crater, Mars. *Geophys. Res. Lett.* 45 (18), 9471–9479. doi:10.1029/2018GL078972

Wiggs, G. F., Livingstone, I., and Warren, A. (1996). The Role of Streamline Curvature in Sand Dune Dynamics: Evidence from Field and Wind Tunnel Measurements. *Geomorphology* 17 (1-3), 29–46. doi:10.1016/0169-555x(95)00093-k

Wilson, I. G. (1971). Desert Sandflow Basins and a Model for the Development of Ergs. *Geographical J.* 137 (2), 180–199. doi:10.2307/1796738

Zgheib, N., Fedele, J. J., Hoyal, D. C. J. D., Perillo, M. M., and Balachandar, S. (2018a). Direct Numerical Simulation of Transverse Ripples: 1. Pattern Initiation and Bedform Interactions. *J. Geophys. Res. Earth Surf.* 123 (3), 448–477. doi:10.1002/2017jf004398

Zgheib, N., Fedele, J. J., Hoyal, D. C. J. D., Perillo, M. M., and Balachandar, S. (2018b). Direct Numerical Simulation of Transverse Ripples: 2. Self-similarity, Bedform Coarsening, and Effect of Neighboring Structures. *J. Geophys. Res. Earth Surf.* 123 (3), 478–500. doi:10.1002/2017jf004399

Conflict of Interest: The authors declare that the research was conducted in the absence of any commercial or financial relationships that could be construed as a potential conflict of interest.